Evaluation of error in temperature starting from the Slit Response Function and the calibration curve of a thermal focal plane array camera

Olivier Riou, Jean Félix Durastanti, Vincent Tortel

Conference paper: Quantitative Infrared Thermography, Padova – Italy (2006)

Evaluation of error in temperature starting from the Slit Response function and calibration curve of a thermal focal plane array camera

Olivier RIOU, Jean Félix DURASTANTI, Vincent TORTEL

Centre de recherche en thermique et environnement des systèmes – CERTES, IUT de Sénart-Fontainebleau, Université Paris XII, Avenue Pierre Point, 77127 Lieusaint, France

Corresponding author: **olivier.riou@u-pec.fr**

Version: **Sunday, September 3, 2023**

Abstract. The sector of the thermographic control of the electric installations is a large user of thermal cameras. This sector has a very large variety of cameras of which image quality is an asset. However, it is not enough to guarantee an exact measurement of temperature. In this work, we give an advanced reading of the Slit response function. It enables us to quantify the systematic error in temperature for a wire-shape object at the T_1 temperature for any wire cross dimension d and back side radiometric temperature T_0, relative to target-camera distance D and using a thermal focal plane array camera. The procedure is detailed and a result obtained on a commercial camera is shown.

http://dx.doi.org/10.21611/qirt.2006.025

1. Introduction

For thermal focal plane camera, we can classify the characteristics of the thermal cameras in two distinct application fields [1]: imagery (the camera provides images) and measurement (the camera is a radiometric apparatus). This is why French standard treats about two resolutions: The Spatial Resolution of Observation or PRSO and the Spatial Resolution of Measurement or PRSM.

A fine analysis of the process of formation of the images shows the limits for spatial resolution. A study of the scattered spot indicates a very strong sensitivity with the numerical aperture NA and the camera's spectral band $\Delta\lambda$. Applied to the focal plane array (FPA) cameras. the spot of diffusion is associated with the impulse response function $\mathrm{D(x)}$ of a detector. In this formalism, we will then be able to give an interpretation of the signal provided by the observation of a slit presenting a strong thermal contrast (SRF for Slit Response Function). Such test will be detailed in connection with the exactitude in temperature. One will point out the characterization of spot to size ratio (SSR) very useful in pyrometry but new in thermography. In this article, one will call upon the French standards of thermography [2]. Nevertheless, FPA cameras being posterior to the standards, those became incomplete and sometimes unsatisfactory. The metrological aspects will be treated in the respect of the International Vocabulary from Metrology or VIM [3].

2. Numerical aperture (NA), f-number (N) and focus

The numerical aperture (NA) of an optical system is a dimensionless number that characterizes the range of angles over which the system captures the irradiance.

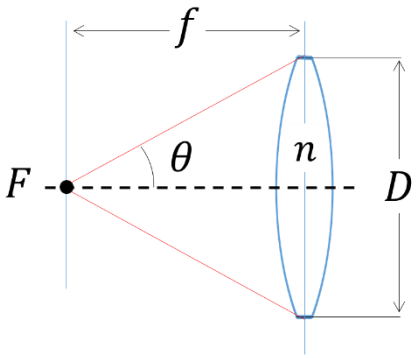

Figure 1. Numerical aperture of a thin lens: $\mathrm{NA} = \mathrm{n} \times \sin(\theta)$. n is the refractive index of the lens' material.

The NA is important because it indicates the spatial resolution of a lens. The size of the finest detail that can be resolved is proportional to $\lambda/2\,\mathrm{NA}$, where λ is the wavelength of the monochromatic irradiance. A lens with a larger NA will be able to visualize finer details than a lens with a smaller NA. Assuming high quality optics with less diffraction effect, the lenses with larger NA will collect more irradiance and generally provide a brighter image but shallower depth of field. Increasing the magnification and NA of the lens reduces the distance between the lens and the target.

The angular aperture of a lens is expressed by the f-number, written f/N, where N is the f-number, which is the ratio of the focal length f to the diameter of the pupil D:

$$\mathrm{N} = \mathrm{f/D} \approx 1/2\mathrm{NA} \qquad (1)$$

http://dx.doi.org/10.21611/qirt.2006.025

The approximation holds when NA is small, but it turns out that for well-corrected optical systems, such as camera lenses, a more detailed analysis shows that the relationship remains nearly true even at large NA.

With regard to thermal defocus, it is important to note that the focal plane of a non-thermalized lens varies with temperature. The quality degradation will be noticeable as soon as the defocus exceeds the depth of field of the camera, which is defined by the aperture of the system and the size of the detector or its image in the focal plane of the lens if a scanning module is used. For example, in the case of lenses with a thermal modular scanning system (SMT) open to F/4.1, the image of the detector in this focal plane has dimensions of 90 µm. It can then be shown that a defocus of the order of 280 µm produces a 10% drop in the modulation transfer function, which is a quality function, with little effect on image quality. Therefore, the lens can be considered athermally printable if the defocus does not exceed this value at extreme operating temperatures [4].

3. Spatial resolution of observation (PRSO)

In imaging, it is useful to define the Spatial Resolution of Observation (PRSO) in terms of the number of detectors, whereas the standard specifies it in terms of an angle. Thus, the PRSO is the product of the number of detectors in a row ($\mathrm{m_{hz}}$) and the number of detectors in a column ($\mathrm{n_v}$): for example, $\mathrm{m_{hz}} \times \mathrm{n_v} = 320 \times 240$.

Due to the non-standard size of the matrices, the field of view (FOV) is the angle from which the camera views the thermal scene. The FOV is an angle that characterizes the spatial extent of the observation. We define the horizontal field of view (HFOV) and the vertical field of view (VFOV).

In geometrical optics, a detector of the FPA sees an elementary area δA of the thermal scene under an angle called the instantaneous field of view (IFOV).

The different fields of view are shown in Figure 2.

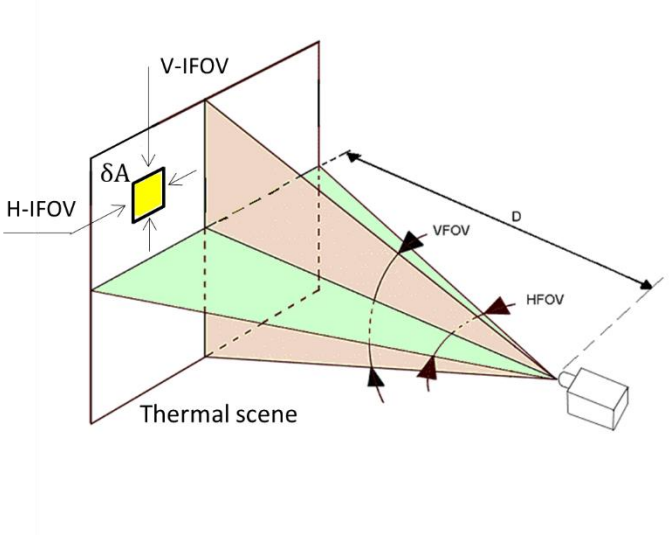

Figure 2. Angles FOV and IFOV. The element area δA is viewed by a square Pel [5]

For practical reasons, the FOV is expressed in angular degrees (°) and IFOV is expressed in milliradians (mrad) or millimeters at measurement distance D (mm @ Dm). IFOV values in mrad or mm @ 1 m are identical. So we have:

$$\mathrm{IFOV[mrad]} = 1000 \times \left(\mathrm{HFOV}\ [°] \times \frac{\pi}{m_{hz} \times 180°} = \mathrm{VFOV}\ [°] \times \frac{\pi}{n_v \times 180°}\right) \qquad (2)$$

Thus, the PRSO of a camera with a HFOV = 18° lens and a 160 x 120 detector matrix can also be expressed by the value of the $\mathrm{IFOV} \approx 2\ \mathrm{mrad}$, or $2\mathrm{mm}\ @\ 1\mathrm{m}$ or $2\mathrm{mm} \times D_f(\mathrm{m})\ @\ D_f(\mathrm{m})$ where D_f is the minimum focusing distance of the camera.

4. Limits of the spatial resolution of focal plane array camera

The nature of the irradiance imposes a limit on the spatial resolution of observation. Mainly because of the phenomena of diffraction and aberration, the image of a point is not a point. These phenomena degrade the spatial resolution of observation of any optical systems and thus the accuracy of irradiance measurement.

The diffraction and the geometric aberrations are physical phenomena present in any systems using pupils (lens. diaphragm…). This phenomenon transforms the image of a point into a scattering spot. The following figure parametrizes the optical system:

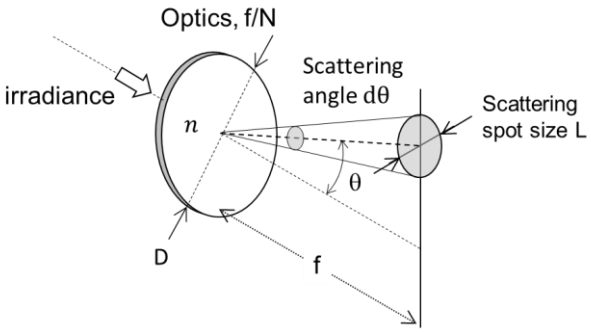

Figure 3. An f/N aperture optics captures an irradiance. Its diameter D produces a scattered spot of size L in its focal plane. n is the refractive index of the thin lens

The size of the scattering spot depends mainly on the f-number N. Since the phenomena are antagonistic, the deformations could be corrected. The processes of correction are well known to opticians. In some simple cases, it is possible to control the size of the scattering spot $L \approx f \times d\theta$.

4.1. Diffraction spot

The diffraction pattern obtained with a circular pupil is rotationally symmetric, with a central amplitude maximum surrounded by rings of zero amplitude alternating with rings of low and decreasing amplitude.

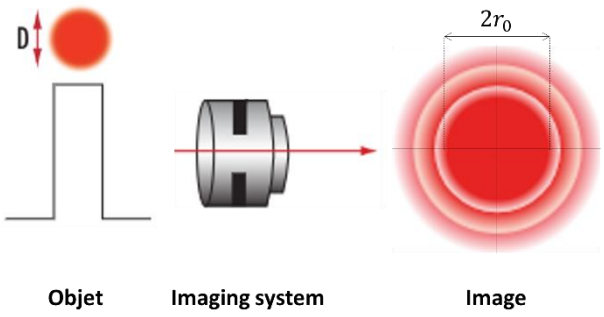

Figure 4. diffraction pattern produced by an imaging system of f-number N

Since the central maximum contains almost all the radiation, the diameter of the first dark ring $2r_0$ gives the image spot size. It is defined by the first zero of the first order Bessel function:

$$L_{scatt.} = 2.44 \times \lambda \times \frac{f}{D} = 2.44\,\lambda\,N \tag{3}$$

Note that this value increases with the f-number N.

4.2. Chromatic aberration

Chromatic aberrations are due to variations in the refractive index of materials with wavelength. These variations directly affect the focal length of the system, which takes on different values depending on the values of λ.

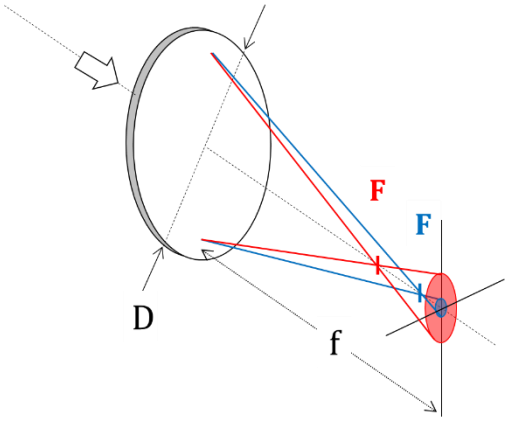

Figure 5. Chromatic axial aberration. An optical system with a f-number f/D produces a scattering spot resulting from variations in the focal length of the system as a function of the wavelength of the irradiation.

For a thin lens, the dispersion $df/d\lambda$ of focal length f with wavelength is quantified by its Abbe-number (or constringency) η. The diameter of the scattering spot in the focal planes corresponding to the two extreme wavelengths is given by [6]:

$$\frac{df}{d\lambda} = -\frac{(dn/d\lambda) \times f}{n-1}$$
$$\left|\frac{\delta f}{f}\right| = \frac{1}{\eta} \tag{4}$$
$$L_{scatt.} = \frac{D}{2\eta}$$

This term is much greater than the diffraction spot. For smaller apertures (f/1 or less), the chromatism can be so large as to make observation impossible. There are, of course, several ways to reduce this aberration. Axial and lateral chromatic aberration is corrected by combining several lenses so that the dispersion of one lens compensates for the dispersion of the others. The corrected system is called achromatic or apochromatic (higher order chromatic corrections). Mirrors are not affected by chromatic aberration.

4.3. Geometric aberrations

The geometric aberrations occur when off-axis rays do not converge at the same point as paraxial rays due to the deviations from the Gaussian condition. The result is a blurred image, which degrades the image quality.

There are three basic aberrations characterized by a third-order development of the transverse geometric aberration: spherical aberration, coma, astigmatism.

Concerning the spherical aberration, in the case of a lens with the best shape for an object point on the axis, we find an image spot of angular diameter [6]:

$$d\theta = 6.8\ 10^{-3} \times \frac{n\ (4n-1)}{(2+n)(n-1)^2 N^3} \approx \frac{0.0075}{N^3} \qquad (5)$$

Coma and astigmatism mainly affect the edge shape of the image in the focal plane. The Coma produces a scattering spot that is not rotationally symmetric. The resulting image is a sliding of circular spots (radius ρ_c) over the distance $\approx 3\rho_c$ [6, 7]. The astigmatism term is proportional to the optical aperture and also occurs in small aperture systems. The field curvature results from deviations from Abbe's law. When affected by astigmatism, the beam has two thinning zones near the image. These zones, called "astigmatic foci", are represented by two small orthogonal segments, T' and S', where the beam is reduced to a brush. The distance T'S' is called the astigmatic distance. In the middle of T'S' is a zone where the image spot is approximately circular. Its size corresponds to the circle of least scattering C'. Outside of C', the spot is elliptical. These ellipses gradually become circles as they move away from the focal zone [8].

4.4. summary

The following table synthetizes the limits of the spatial resolution of infrared camera.

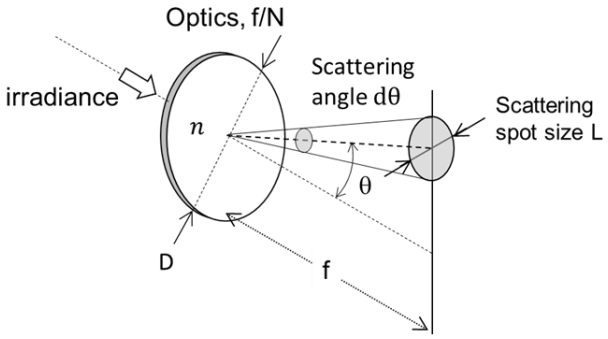

Parameters:	Thin lens of best shape (refractive index n, Abbe-number η) F-number $N = f / D \approx 1 / 2NA$ Scattering diameter $L \approx f \times d\theta$ in the Gauss conditions
Angular diameter of the diffraction spot [mrad] :	$d\theta = \frac{2.44 \times \lambda}{D}$
Angular diameter of the chromatic spot [mrad] :	$d\theta = \frac{1}{2\eta N}$
Angular diameter of the spherical aberration [mrad] :	$d\theta = 6.8\ 10^{-3} \times \frac{n\ (4n-1)}{(2+n)(n-1)^2 N^3}$
Coma [rad]	$\theta_c = \frac{\theta}{16(n+2)N^2}$
Angular diameter of the Astigmatism [mrad]:	$d\theta = \frac{\theta^2}{2N}$

Table 1. Scattering angles

5. Discussion in the case of thin lens of germanium

Germanium optics are widely used in infrared thermography because of their high transmittance which covers the MWIR and LWIR bands ($\tau_{3-12\mu m} > 90\%$) and of its high refractive index ($n \approx 4$) which is an advantage for reducing spherical aberration (Eq. 5). The refractive index temperature coefficient of germanium is of order of 0.000396/°C. This value is large and may produce a large focal shift during the lens temperature change (section 2).

It is interesting to compare the spatial resolution performance of a single lens in the MWIR spectral bands [3µm; 5µm] and the LWIR band [8µm; 12µm]. We then evaluate the scattering spot size in the case of a thin germanium lens. The pupil diameter is arbitrarily set to D=50 mm, and the focal length is f=100 mm, resulting in the f-number N=2 commonly found in commercial cameras.

The optical properties of the lens are its refractive index n and its Abbe number η. The refractive index value is found to be constant n≈4 within both the MWIR and LWIR bands. The Abbe number varies with the spectral band. Concerning the MWIR band ($\bar{\lambda} = 4\mu m$), we quantify its value according to the relation $\eta_{\Delta\lambda}^{-1} = \delta f/f \approx (dn/d\lambda \times \Delta\lambda)/(\bar{n} - 1)$ (**Eq. 4**). The characteristic $n(\lambda)$ can be found in the literature [9]. The calculation leads to $\eta_{3-5} \approx 110$ at 293K. For the LWIR band ($\bar{\lambda} = 10\mu m$) a convergent value of $\eta_{8-12} \approx 1112$ (293K) is found [4, 10]. Note that the chromatism is more pronounced in the MWIR band than in the LWIR, because the dispersion $dn/d\lambda$ is important.

Spectral band	MWIR		LWIR	
designation	Scatering angle θ	Scatering spot size L	Scatering angleθ	Scatering spot size L
unity	mrad	mm	mrad	mm
Diffraction	0,1952	0,02	0,49	0,049
Chromatic	5	0,5	0,22	0,022
Spherical aberration	0,9	0,09	0,9	0,09
Coma (image edge)	0,6	0,1	0,6	0,1
Astigmatism (image edge)	15	1,5	15	1,5

Table 2. Scatter spot evaluation for a thin germanium lens

This example shows that PRSO is strongly limited by the quality of used lens. specially at the edge of the images where the coma and the astigmatism are dominant. At the center of image and for an achromatic optics, the scattering angle cannot be less than 1.4 mrad for an optic number of f/2 in the LWIR band. It is not rare to meet cameras of optic number greater (f/1). For such cameras, the scattering angle is strongly increased. Additional chromatic correction is required in the case of MWIR cameras, resulting in more expensive optical systems compared to LWIR cameras.

These limitations are obviously managed by the camera manufacturers. Assuming a standard correction of 90%, the scattered spot size, including chromaticity and aberrations, varies from 26µm to 80µm. This makes it impossible to accurately quantify the irradiance of an object spot viewed by a single detector (i.e., one IFOV, Fig. 2) since its typical size is in the order of 10µm to 45µm respectively, regardless of the spectral band of detection. The use of large diameter pupils could be reducing these limits but it significantly increases the footprint of the system.

http://dx.doi.org/10.21611/qirt.2006.025

6. Impulse Response

All these optical limits are synthetized into the linear impulse response $D(x)$ of the optical system. One models the impulse response by a Gaussian function in which σ_x represents the scattering length :

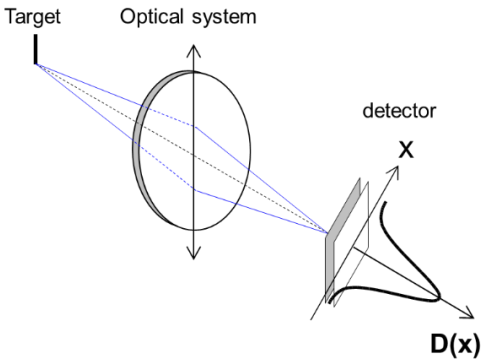

Figure 6. Linear impulse response of an optical system

$$D(X) = D_0 e^{-X^2/2\sigma_x^2} \tag{6}$$

Focal plane array thermal imagers are designed to meet two conflicting requirements. On the one hand, the thermal image must be as sharp as possible, which requires miniaturization of the detectors and densification of the detector matrix. On the other hand, the quantification of the irradiance by a detector must be as accurate as possible, which fits the detector size d to the Gaussian scattering size σ_x.

The impulse response function is useful to determine relationship between the scattering spot size and the effective detector one:

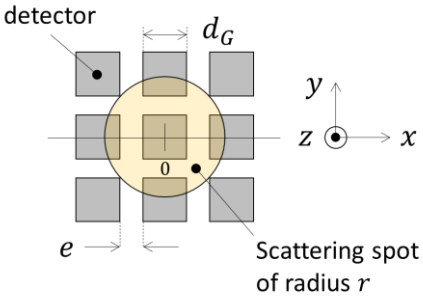

Figure 7. Detectors in a focal plane array. The effective detector size is $d = d_G + e$, while the scattering spot is spread over a diameter of $2r$. The intensity of the irradiance within the scattering spot is modeled by a 2D Gaussian function together with its scattering radius σ_r.

Note that the intensity of the flux in nonlinear along the X-direction and Y-direction. The Gaussian distribution is symmetrical along the Z-direction. Given a scattering spot of characteristic radius σ_r and detector size d, we can determine the number of detectors the spot must cover to ensure accurate quantification of the irradiance by at least one of them. This is done by optimizing the ratio of the quantifiable flux over a length x to the scattered flux one which defines the spread function (SF):

$$SF(u) = \frac{\int_{-u}^{u} e^{-X^2/2} dX}{\int_{-\infty}^{+\infty} e^{-X^2/2} dX} \tag{7}$$

The length x is arbitrarily set to $i \times d$ when $\pm u = x/\sigma_r = (i-1) + 0.5$ ($i \in \mathbb{N}_0^+$), i.e. $d = \sigma_r$. Some particular values of the spread function are presented in figure 8.

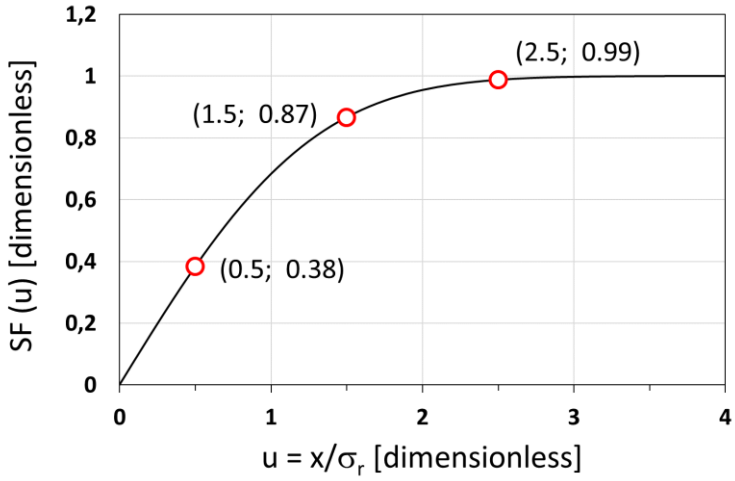

Figure 8. Evaluation of spread function versus $u = x/\sigma_r$.

When $d \approx \sigma_r$, the flux quantified by one central detector is only 38% of the total irradiance. Full accuracy is achieved when $5 \times d \approx \sigma_r$: the scattered spot size covers five detectors, which the central detector gives a flux quantification of 99%

7. Slit Response Function (SRF)

The SRF test is very useful when one wants to clarify the precautions to be taken for an accurate irradiance measurement of a slim line target shape of thickness t. To carry out the test, we usually use an adjustable slit (Figures 9a and 9b).

for most cases, thermal Cameras are designed to measure the radiation linearly: Each detector provides a thermosignal $L_{\Delta\lambda}$ proportional to the irradiance. As the slit aperture t decreases, and below a certain value, the thermosignal starts to decrease from $L_{\Delta\lambda}(T_1)$ to $L_{\Delta\lambda}(T_0)$. For each slit aperture, the normalized camera response is therefore:

$$SRF = \frac{L_{\Delta\lambda}(T_{app}) - L_{\Delta\lambda}(T_0)}{L_{\Delta\lambda}(T_1) - L_{\Delta\lambda}(T_0)} \qquad (7)$$

The scattered spot results from the optic path followed by the irradiance. Its magnitude depends on the technological choices made by the camera designer, in particular the pupil diameter, the focal length and the working spectral band. On the other hand, it does not depend on the quantization of the irradiance by the detectors. The shape of the SRF should then be preserved, regardless of the irradiance intensity.

The SRF remains unchanged regardless of $L^0_{\Delta\lambda}(T_1)$ and $L^0_{\Delta\lambda}(T_0)$, so the slit and black body can be brought to any temperature. The contrast $T_1 - T_0 \geq 30°C$ optimizes the accuracy of the SRF. To be valid, the test must be performed without changing the temperature range of the camera. The influence temperatures must be kept as stable as possible, which poses the problem of the black body stability (dT_1/dt), of the self-heating of the slit exposed to the black body radiance (dT_0/dt) and of the thermal drift of the camera ($dT_{app.}/dt$). Under these conditions, it is quite easy to quantify the SRF versus t, or $\alpha = t/D$. However, micrometric adjustments should be made to align a detector column to the slit and find the maximum camera response using the "maximum on profile" function.

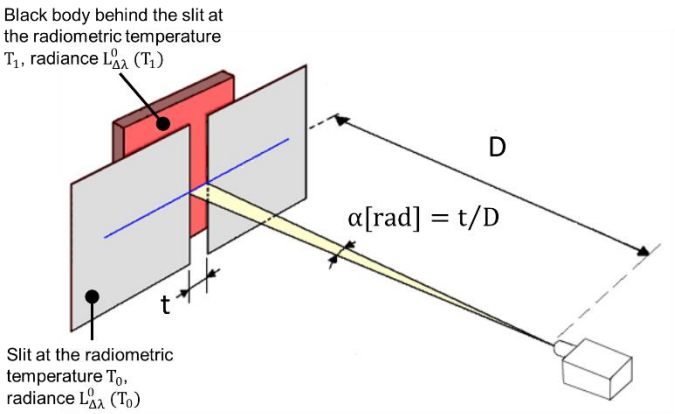

Figure 9a. Slit response function. The camera sees a slit temperature T_0 (front face radiometric temperature) and the black body behind the slit at radiometric temperature T_1 (line temperature). The slit aperture is d and D is the distance from the slit to the camera. The line is viewed through $\alpha = t/D$. $\Delta\lambda$ is the spectral bandwidth of the camera. Infographic is issue from [**5**].

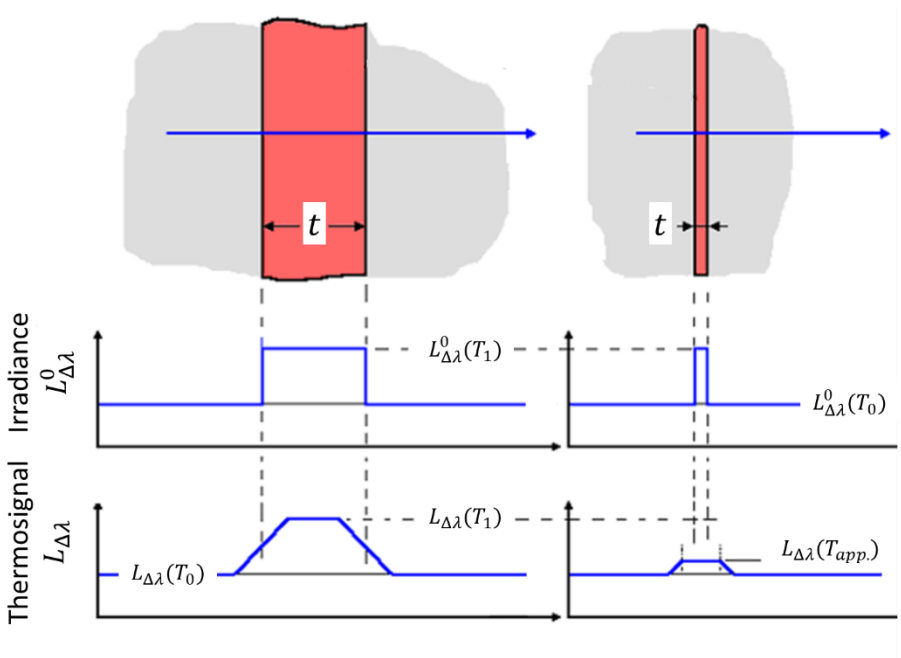

Figure 9b. The irradiance is quantified by the black body luminance in $\mathrm{W\,m^{-2}\mu m^{-1}sr^{-1}}$ unity. The thermosignal delivered by the camera is denoted $L_{\Delta\lambda}(T_{app.})$ in level unity. Infographic is issue from reference [5].

8. Exactitude in apparent temperature

When we treat the apparent temperature accuracy, the system must be characterized in terms of repeatability (type-A uncertainty) and reproducibility (type-B uncertainty). To quantify exactitude in temperature, it is necessary to give to the object an angular dimension $\alpha = t/D$ which makes the SRF within the range $[1; 1-\varepsilon]$ (ε is the systematic error in measurement). A variation of ε% on the relative value of the signal corresponds to a systematic error in temperature given by the relation 8:

$$\Delta T_{bb} = \frac{L_{\Delta\lambda}(T_1) - L_{\Delta\lambda}(T_{app.})}{s} \qquad (8)$$

where $\Delta L_{\Delta\lambda}$ is the level variation on the SRF and s is the camera sensitivity in $\mathrm{Level}/°\mathrm{C}$ at temperature T_1. The systematic error ΔT_{bb} is generally negative because the black body temperature is estimated by default when $T_1 > T_0$. The sensitivity is derived from the camera calibration curve. The systematic error ΔT_{bb} then depends on the black body temperature T_1, on the slit temperature T_0 and on the distance to size ratio t/D. The systematic error ΔT_{bb} then depends on these parameters.

The analysis is given for a vertical slit arrangement. The test may be worse in a horizontal arrangement or if the object is disk-shaped. It is therefore equally important to produce the test results in these arrangements and to agree on the choice of a test in the most unfavorable situation [11].

9. Application

Let's take a bolometric thermal camera 320×240 ($\mathrm{IFOV} = 2.1\ \mathrm{mrad}$), whose spatial resolution is based on observing the signal from a high thermal contrast vertical slits. The slits are backward illuminated by a black body whose temperature is set at 70°C. The emitting slits are at the temperature of 20°C. They are positioned at the minimum focusing distance of the camera, i.e. D=30 cm. The angular observation aperture is defined by the ratio t/D, where t is the slit aperture. The test is performed for standard optics ($24° \times 18°$) after the system stabilization time. The result is shown in Figure 10.

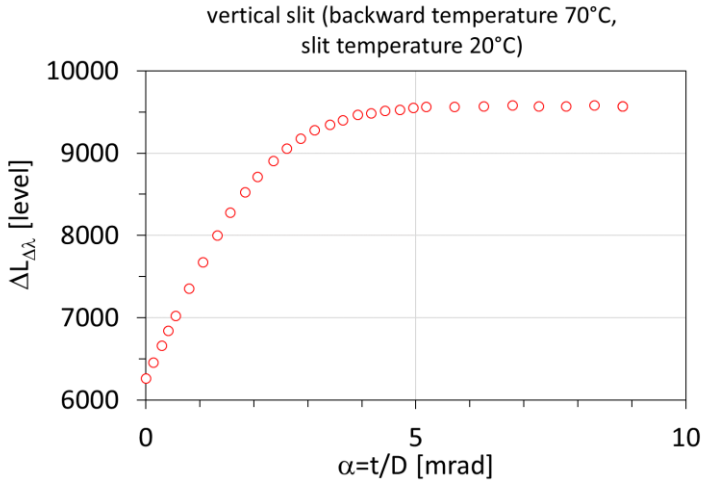

Figure 10. Vertical SRF of a bolometric thermal camera (320×240 detectors, standard optics $24° \times 18°$, $\mathrm{IFOV} = 2.1\ \mathrm{mrad}$). The function is characterized at the focusing distance of D=30 cm.

Using the sensitivity of the camera at 70°C ($s = 66\ \mathrm{levels}/°\mathrm{C}$), we can convert the signal values into temperature. The result is shown in Table 3.

Some specific values are shown in Table 3.

α/IFOV	dimensioneless	1	2	3	4
$\Delta L_{\Delta\lambda}$	Level	830,8	82,5	-1,3	-11,4
Δθ	°C	12,6	1,25	-0,02	-0,2

Table 3. results of SRF using vertical slit at 20°C

The systematic error of the temperature is very large for small apertures. In the opposite case ($t/D > 3\ \mathrm{IFOV}$), it is in the order of the instrumental uncertainty. Projected on the object plane, the characteristic size of the measurement zone at 50 cm is of the order of 2 mm.

http://dx.doi.org/10.21611/qirt.2006.025

One can derive the temperature accuracy for any black body temperature by implementing the SRF from T_0 to T_1. Of course. the study also assumes that the behavior of the camera remains homothetic on the usual distances D of the measurements. In this context, we propose a second reading of the SRF. The protocol is as follows:

1. We measure the SRF for the slit temperature T_0 (for example 20°C) and the black body temperature T_1 (for example 70°C). The normalized SRF of the camera is calculated for each slit aperture t by Eq. 7. The result is expressed in radiometric levels of the level $L_{\Delta\lambda}(T_1)$ and of the level $L_{\Delta\lambda}(T_0)$ as is depicted in Figure 10,
2. Since the SRF remains unchanged regardless of $L^0_{\Delta\lambda}(T_1)$ and $L^0_{\Delta\lambda}(T_0)$, we can computed the value of $L_{\Delta\lambda}(T_{app.})$ using Eq. 7 and the calibration curve of the camera for different slit temperatures varying between 20°C and 70°C by keeping the black body temperature to T_1,
3. We compute the systematic error of the temperature (Eq. 8) by calculating the sensitivity $s(t_{app.})$ for each apparent temperature,
4. The result is finally plotted as a curve of the slit temperature versus the size to distance t/D ratio. The result could be classified taking account of an arbitrary temperature accuracy threshold.

This protocol is applied to a LWIR bolometric thermal camera (320×240 detectors, standard optics $24° \times 18°$, $\mathrm{IFOV} = 2.1$ mrad). The function is characterized at the focusing distance of $D = 30$ cm. The result is showed in figure 11.

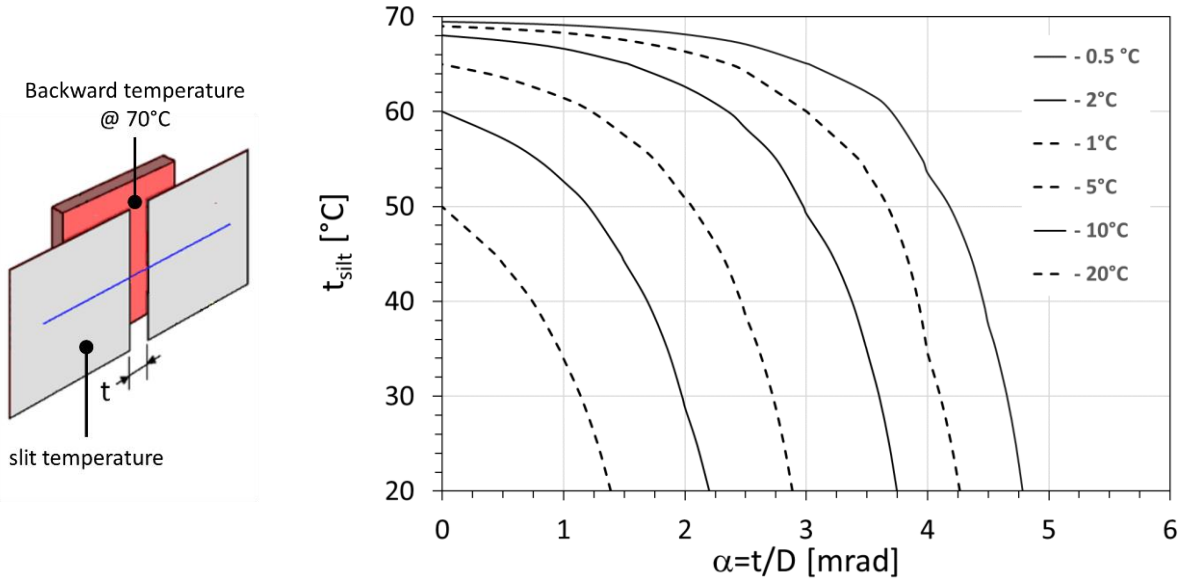

Figure 11. Accuracy of temperature measurement of a slender object in a vertical position (70°C). Amplitude of error is shown in legend.

Suppose that a vertical wire ($T_1 = 70°C$) is observed at a distance of 50 cm in an object radiometric environment of $T_0 = 40°C$. If this wire has a diameter of 2 mm, the ratio of size to distance t/D is $1:250$ or 4 mrad (2.4 IFOV). In the apparent temperature situation, the systematic error should be in the order of $-1°C$. In the case of a vertical wire with a diameter greater than 2.5 mm, the latter should be less than $-0.5°C$, regardless of the object radiometric environment. For a wire covering only 1 IFOV (2.1 mrad or $1:476$), the systematic error range within $[> -10°C; < -0.5°C]$ depending on the slit temperature. Finally, note that if the wire is at the same apparent temperature as the object radiometric environment,

the camera will not resolve it, but the irradiance measurement will be very satisfactory because the temperatures are roughly spatially identical. Then, if the temperature contrast between the wire and the object radiometric environment is enhanced, one will be able to correctly image the wire of small diameters. In imaging, this is not a problem: the camera sees correctly the wire. The IFOV is therefore an image-related concept and does not guarantee the validity of the radiometric measurement.

10. Conclusion

A fine analysis of the infrared imagery process showed the limits of the spatial resolution of the camera. A quantified study of the scattered spot is given and indicates a strong sensitivity with f/N of the camera and its spectral band. This limits reduce the exactitude in temperature. We propose a second reading of the signal provided by the observation of a slit presenting a strong thermal contrast (Slit response function). It should be noted that systematic error of temperature depends of four parameters: the object's temperature, the object shape and orientation, the object radiometric environment and the size to distance ratio t/D. Each influence parameters are studied. Systematic errors are presented on a new single graph providing direct access for any of this parameters. It appears more relevant than current standards.

References

[1] Dominique PAJANI, Luc AUDAIRE (2001). Thermographie - Technologies et applications. https://doi.org/10.51257/a-v2-r2741

[2] Thermographie infrarouge : caractérisation de l'appareillage, NF A 09-420 (1993) et méthodes de caractérisation de l'appareillage, NF A 09-421 (1993)

[3] Essais non destructifs - Thermographie infrarouge - Vocabulaire relatif à la caractérisation de l'appareillage. NF A 09-400 (décembre 1991)

[4] European Patent Office, EP0480805A1 (1990). Systèmes d'objectifs à athermalisation optique

[5] Dominique Pajani (2005). Résolutions spatiales des caméras thermiques à matrice de détecteurs. Thermogram' 2005.

[6] Herbert RUNCIMAN (1995). Aberrations des systèmes optiques : éléments de conception optique. Techniques de l'Ingénieur, E4040 v1. https://doi.org/10.51257/a-v1-e4040

[7] G. Gaussorgues. La thermographie infrarouge : principes, technologies, applications (4ème édition, page 211). ISBN-10 2743002905

[8] G. Gaussorgues. La thermographie infrarouge : principes, technologies, applications (4ème édition, page 160 & 164). ISBN-10 2743002905

[9] Bradley J. Frey, Douglas B. Leviton, and Timothy J. Madison (2006). Temperature-dependent refractive index of silicon and germanium. Proc. SPIE 6273, Optomechanical Technologies for Astronomy, 62732J. https://doi.org/10.1117/12.672850

[10] G. Gaussorgues. La thermographie infrarouge : principes, technologies, applications (4ème édition, page 213). ISBN-10 2743002905

[11] Warren C. Garber. Applying distance to spot ratio values to infrared imagers for accurate temperature measurement. https://irinfo.org/10-01-2002-garber/. The information in this article should be used with caution, as the author does not specify the camera's optical system or the criteria for obtaining results.